

Article

Ferromagnetic Biochar Prepared from Hydrothermally Modified Calcined Mango Seeds for Fenton-like Degradation of Indigo Carmine

Aurelien Bopda ¹, Sandrale Grace Mokue Mafo ¹, Josiane Nguimatsia Ndongmo ^{1,2}, Georges Teikam Kenda ¹, Cyrille Ghislain Fotsop ³ , Idris-Hermann Tiotsop Kuete ¹ , Christian Sadeu Ngakou ¹, Donald Raoul Tchuifon Tchuifon ^{4,*}, Arnaud Kamdem Tamo ^{5,6,7,*} , George Ndifor-Angwafor Nche ^{1,*} and Solomon Gabche Anagho ^{1,*}

- ¹ Research Unit of Noxious Chemistry and Environmental Engineering, Department of Chemistry, Faculty of Science, University of Dschang, Dschang P.O. Box 67, Cameroon
- ² Department of Chemistry, Faculty of Science, University of Douala, Douala P.O. Box 24157, Cameroon
- ³ Institute of Chemistry, Faculty of Process and Systems Engineering, Universität Platz 2, 39106 Magdeburg, Germany
- ⁴ Department of Process Engineering, Laboratory of Energy, Materials, Modeling and Method, National Higher Polytechnic School of Douala, University of Douala, Douala P.O. Box 2701, Cameroon
- ⁵ Laboratory for Bioinspired Materials BMBT, Institute of Microsystems Engineering IMTEK, University of Freiburg, 79110 Freiburg, Germany
- ⁶ Freiburg Center for Interactive Materials and Bioinspired Technologies FIT, University of Freiburg, 79110 Freiburg, Germany
- ⁷ Freiburg Materials Research Center FMF, University of Freiburg, 79104 Freiburg, Germany
- * Correspondence: tchuifondonald@yahoo.fr (D.R.T.T.); arnaud.kamdem@imtek.uni-freiburg.de (A.K.T.); nchegeorges4@yahoo.com (G.N.-A.N.); sg_anagho@yahoo.com (S.G.A.); Tel.: +237-674-780-094 (D.R.T.T.); +49-761-203-95096 (A.K.T.); +237-677-504-573 (G.N.-A.N.); +237-677-578-567 (S.G.A.)



Citation: Bopda, A.; Mafo, S.G.M.; Ndongmo, J.N.; Kenda, G.T.; Fotsop, C.G.; Kuete, I.-H.T.; Ngakou, C.S.; Tchuifon, D.R.T.; Tamo, A.K.; Nche, G.N.-A.; et al. Ferromagnetic Biochar Prepared from Hydrothermally Modified Calcined Mango Seeds for Fenton-like Degradation of Indigo Carmine. *C* **2022**, *8*, 81. <https://doi.org/10.3390/c8040081>

Academic Editor: Manuel Fernando Ribeiro Pereira

Received: 31 October 2022

Accepted: 13 December 2022

Published: 19 December 2022

Publisher's Note: MDPI stays neutral with regard to jurisdictional claims in published maps and institutional affiliations.



Copyright: © 2022 by the authors. Licensee MDPI, Basel, Switzerland. This article is an open access article distributed under the terms and conditions of the Creative Commons Attribution (CC BY) license (<https://creativecommons.org/licenses/by/4.0/>).

Abstract: Biochar and ferromagnetic biochar obtained from the pyrolysis of dried mango seeds and modified using a hydrothermal method were used as catalyst for the heterogeneous degradation of indigo carmine in an aqueous medium. These prepared biochars were characterized using different techniques: Fourier transform infrared spectroscopy (FTIR), X-ray diffraction (XRD), scanning electron microscopy (SEM) and energy dispersive X-ray spectroscopy (EDX). The analyses of the results revealed the presence of iron oxide in the form of magnetite (Fe₃O₄) in the catalyst. The catalytic tests carried out with this composite material showed a significant degradation of indigo carmine. The maximum degradation of indigo carmine in the aqueous solution was reached after 240 min of agitation. The Fenton degradation process using irradiation with a 100 W electric lamp and hydrogen peroxide (concentration 4 mol/L) showed the best results at pH = 3. From this study, it emerged that the second-order kinetic model better described the degradation process, and it gave lower half-lives compared to those obtained with the first-order kinetic law. The study also showed that ferromagnetic biochar could be prepared from mango seeds and used for the degradation of indigo carmine in an aqueous solution.

Keywords: ferromagnetic biochar; indigo carmine; Fenton process; hydrothermal method

1. Introduction

The expansion of anthropogenic activities inevitably leads to discharges of effluents laden with several toxic chemicals into the environment. These effluents contain various compounds such as heavy metals, pesticides and dyes, and they appear in dissolved or insoluble forms. These chemicals currently occupy an important place in the industrial sector. They are widely used in the paper, cosmetic, food and textile industries [1–5]. The continued release of these recalcitrant compounds into the environment leads to long-term

accumulation in the ecosystem. Once released and accumulated in different environments, these potentially toxic substances can be absorbed by living organisms, accumulate in biological tissues and harm the health of living organisms in the polluted environment [6,7]. In addition, the interactions between these polluted ecosystems and living beings lead to harmful effects, given the nuisances that these pollutants can cause. Some of these substances, which bioaccumulate in plants, animals and humans, are known to be toxic, carcinogenic, teratogenic or cause death, sterility or malformations [8].

As an example, indigo carmine of the indigoid family is considered one of the toxic environmental pollutants. It is used as a dye in the textile industry; it is also used as a color indicator in analytical chemistry. However, according to the World Health Organization, its concentration limit in water intended for human consumption is 0.005 mg/L. Beyond this dose, it is considered toxic and can cause gastrointestinal disorders characterized by nausea, vomiting and diarrhea upon ingestion [9,10].

Faced with the dangers posed by this dye, the search for solutions has led to the development of methods such as adsorption, flocculation/coagulation and chemical oxidation for its elimination in effluents [1,2,11,12]. However, techniques such as adsorption and flocculation can be very limited because some pollutants still persist in the medium after treatment [13]. Chemical oxidation has also shown a limited capacity in the face of the complexity of certain pollutants. Thus, new treatment processes have emerged over the past 20 years, including advanced oxidation processes (AOP), which have proved to be very interesting for the degradation of recalcitrant organic molecules. Advanced oxidation aims at the complete mineralization of aqueous pollutants into CO₂, H₂O and other mineral ions [10]. These processes are based on the formation of very reactive and non-selective radical entities such as OH[•], which have a very high oxidizing power ($E^{\theta} = 2.8 \text{ V}$) [14]. The AOP used in this study is the Fenton process.

The Fenton process, which is one of the advanced oxidation processes, is a method that has proven to be effective in the elimination of a significant number of organic pollutants from wastewater [15,16]. This process essentially uses Fe²⁺ and H₂O₂ to generate highly reactive OH[•] capable of oxidizing even the most persistent organic compounds. In addition, hydrogen peroxide is a powerful oxidant, which also has the particularity of being able to act as a reducing agent under certain conditions. Hydrogen peroxide is one of the strongest oxidants known to be stronger than chlorine, chlorine dioxide and potassium permanganate [17]. Through catalysis, H₂O₂ can be converted into hydroxyl radicals (OH[•]) with a reactivity second only to fluorine. Also, the stability of H₂O₂ is much less due to the presence of an O–O bond or a peroxide bond as shown in the structure. This tendency makes H₂O₂ a better oxidizing agent compared to water, which is more stable due to its hydrogen bonds. Hydroxyl radicals are produced from the catalytic decomposition of H₂O₂ by ferrous or ferric salts. This process uses relatively inexpensive and non-toxic reactants and catalysts and has great potential for industrial applications [18,19].

In order to reduce the cost linked in particular to iron intake, it may be interesting to turn to local materials such as mango seeds transformed into ferromagnetic biochar, which is rich in iron and could be used as an iron substitute. Today, there are several methods to immobilize iron in the form of oxides on a biochar support, namely the hydrothermal method, the co-precipitation technique and the sol-gel method [20,21]. The hydrothermal method is the most commonly used because it is easy to implement and it takes place at relatively lower temperatures. This technique is probably the simplest and most convenient chemical route to synthesize magnetic nanoparticles. The hydrothermal method consumes less energy, thanks to non-extreme reaction temperatures on the one hand. On the other hand, it allows the use of simple and inexpensive chemicals. As the temperature in the hydrothermal treatment is low, the reactions occur very quickly and yield crystalline products [22,23]. Considering the advantages offered by the hydrothermal method for the synthesis of a robust catalyst containing iron oxides that can be effectively used for the treatment of contaminated water, this method was chosen and employed for the functionalization of the precursor biochar obtained by pyrolysis of biomass feedstocks (mango

seeds). Based on the abundant sources of biomass feedstocks and flexible preparation processes, biochar with various functions can be developed and used in various processes of degradation and mineralization of water pollutants. In addition, the recovery of this agricultural waste by pyrolysis to obtain carbonaceous materials is generally performed in closed furnaces with or without the presence of a very small amount of oxygen. This has the advantage of limiting air pollution through the release of greenhouse gases into the environment [24–27]. In addition to what was mentioned above, in a context where the shortage of digestible water for consumption or for urban and domestic work is increasingly felt in developing countries, this study is part of the implementation of an economical process for wastewater treatment, which is essential for recycling useful water for other cost-effective activities.

In this study, biochar was prepared from dried mango seeds using simple pyrolysis. Subsequently, the hydrothermal method was used for the immobilization of iron in the previously prepared biochar. The prepared ferromagnetic biochar as well as the precursor material (non-modified biochar) were characterized by various techniques, such as Fourier transform infrared spectroscopy (FTIR), X-ray diffraction (XRD), scanning electron microscopy (SEM) and energy dispersive X-ray spectroscopy (EDX) analysis. The ability of the particles to facilitate the Fenton oxidation of indigo carmine was also studied under different pH, H₂O₂ concentration and light intensity conditions. The kinetics of the indigo carmine degradation were also modeled using kinetic models already described in the literature in order to define the kinetic parameters related to the catalysis or degradation processes involved.

2. Materials and Methods

2.1. Materials and Chemicals

The mango (*Mangifera indica*) seeds used in this study were collected from the town of Foubot, in the Noun Division of the West Region of Cameroon. Iron (II) sulfate heptahydrate (FeSO₄·7H₂O, purity 99%) was purchased from Sigma Aldrich (Schnellendorf, Germany), sodium hydroxide (NaOH, purity 97%) from Fischer Scientific (Waltham, MA, USA), hydrogen peroxide (H₂O₂, 50%) from PROLABO and indigo carmine (IC) (C₁₆H₈N₂Na₂O₈S₂, 98%) from Sigma Aldrich.

2.2. Preparation of Non-Modified Biochar (BNM) and Ferromagnetic Biochar (BNMF)

The collected mango seeds were washed with water and dried in the sun and preserved to be used as precursor in the preparation of the biochars. To prepare the non-modified biochar, 50 g of mango seeds were packed in closed ceramic crucibles to limit their exposure to oxygen. The crucibles were then placed in an ISUNU furnace and pyrolyzed at 450 °C for 1 h. After cooling to room temperature, the biochar obtained was ground with a porcelain mortar and sieved to obtain biochar particles of sizes ≤ 1000 μm. This resultant product was called non-modified biochar and was coded BNM.

Ferromagnetic biochar was then prepared from the non-modified biochar using the following hydrothermal method: 10 g of non-modified biochar (BNM) was introduced into 250 mL of an aqueous solution containing 5 g of NaOH and 30 g of FeSO₄·7H₂O. The mixture was subjected to magnetic stirring at 80 °C for 2 h. The resulting mixture was then filtered, and the residue washed several times with distilled water until the pH of the supernatant collected from the washing corresponded to the pH of the initial distilled water. The residue was first dried in air, and then in the oven set at 105 °C for 24 h to obtain ferromagnetic biochar (BNMF). It was stored in a desiccator for further use.

2.3. Material Characterization

The non-modified biochar (BNM) and the ferromagnetic biochar (BNMF) were characterized using physico-chemical techniques.

To determine the pH at the point of zero charge (pH_{pZC}), 30 mL of sodium chloride (NaCl) solution with a concentration of 0.1 mol/L was put into different vials and the pH

was adjusted from 2 to 12 using a 1 mol/L solution of NaOH or HCl, and the values noted and called initial pH. A total of 100 mg of the biochar was then added into each vial and the suspensions were stirred for 24 h. After stirring, the resulting solutions were filtered using filter paper and the pH values of the filtrates were read and called final pH. From the plots of the final pH as a function of the initial pH, the pH_{PZC} for the corresponding biochar was obtained as the intersection between this curve and the bisector of the first quadrant.

To determine the pH of the biochar material, 30 mL of distilled water was put in contact with 100 mg of the biochar in a conical flask. The mixture in the flask was shaken for 24 h. Finally, the suspension was filtered and the different pH values of the filtrates read using a pH meter.

The functional groups present in the BNM and BNMF materials were determined by Fourier transform infrared spectroscopy (FTIR). A Nicolet IS5 Thermoscientific Infrared Spectrophotometer was used. The reflection attenuation (RTA) method was used. Recording was performed using a Nicolet IS5-TF spectrophotometer. For each run, the germanium surface was cleaned with methanol, then a few milligrams of the biochar was deposited on the measuring surface consisting of a diamond crystal. After covering the sample with a device integrated into the apparatus, the recording of the spectra of the material and of the blank was carried out.

The X-ray diffraction analysis of the two materials, BNM and BNMF, was performed using an automated PAN XPERT Pro analytical powder diffractometer with anode-filtered Cu-K radiation. The samples were scanned with an accelerating voltage of 40 kV, a radiation wavelength, $\lambda = 1.5406 \text{ \AA}$, a current of 40 mA and a 2θ range between 4° and 65° .

The EDX and SEM analyses were performed using a JEOL JSM-6390A (Tokyo, Japan) scanning electron microscope at an accelerating voltage of 10 kV. Prior to measurement, the samples were coated with a thin layer of sputtered gold to increase their conductivity.

2.4. Experimental Procedure for the Degradation of Indigo Carmine in Aqueous Solution

To evaluate the catalytic activity of the prepared biochar materials, 100 mL of indigo carmine solution (100 mg/L) was brought into contact with 300 mg of the prepared biochars in a conical flask, and 5 mL of H_2O_2 of concentration 17.49 mol/L was added to the mixture. The pH was adjusted using 1 mol/L solution of NaOH or H_2SO_4 . To explore the effect of pH on the Fenton-like reaction and to compare the catalytic degradation of indigo carmine using ferromagnetic biochar (BNMF) as catalyst, several different pH conditions were selected. For degradation studies, the pH of the reaction mixture ranged from 2 to 8. The suspension was stirred using a magnetic stirrer at 100 rpm at room temperature for 240 min in the dark to ensure degradation. At an appropriate time, 5 mL of the suspension containing indigo carmine solution was withdrawn from the conical flask, placed in an ice bath to stop the reaction and then filtered. The absorbance of the filtrate was read from the UV-Vis spectrophotometer at maximum absorption wavelength of 612 nm. Other samples were extracted at defined time intervals ranging from 5 to 240 min and their corresponding absorbance also read (Figure 1). The procedure was repeated but with the suspension exposed to daylight.

The percentage degradation (%R) of indigo carmine was calculated from the following formula:

$$\%R = \frac{C_0 - C_t}{C_0} \times 100 \quad (1)$$

where C_0 (mg/L) is the initial concentration of indigo carmine while C_t (mg/L) is its concentration at the reaction time t .

Kinetic studies were performed using first-order and second-order kinetic models. The indigo carmine bleaching equation (Equation (2)) in solution as well as those corresponding to the different orders of the kinetic models are described below.



For a kinetics of order 1:

$$V = -\frac{dC}{dt} = kC \quad (3)$$

Upon integration (with $C = C_0$ at $t = 0$);

$$\ln \frac{C_t}{C_0} = -kt \quad (4)$$

For kinetics of order 2:

$$V = -\frac{dC}{dt} = kC^2 \quad (5)$$

Upon integration (with $C = C_0$ at $t = 0$);

$$\frac{1}{C_t} - \frac{1}{C_0} = kt \quad (6)$$

where C_0 (mg/L) is the initial concentration of indigo carmine and C_t is the concentration (mg/L) of indigo carmine at a certain reaction time t (min), while k is the reaction rate coefficient (min^{-1}).



Figure 1. Images showing discoloration of indigo carmine solution over time after treatment.

3. Results

3.1. Characterization of Materials

The different functional groups present on the surface of the non-modified biochar (BNM) and the modified biochar (BNMF) were determined using FTIR spectroscopy. The analyses were carried out in the wavelength range from 4000 to 500 cm^{-1} . The infrared spectra are shown in Figure 2.

The FTIR spectra of the two materials, BNM and BNMF, show that in the region between 2550 and 2000 cm^{-1} , peaks characteristic of the aliphatic stretching vibrations C-C appear. We also observe peaks appearing at 1650 cm^{-1} on these spectra that are attributed to the stretching of the carbonyl C=O groups of ketones, aldehydes or lactones. The peak observed at 1025 cm^{-1} is attributed to the C-O ether stretching vibrations [28–32]. There is a significant difference between the two FTIR spectra for BNM and BNMF. This testifies to the effectiveness of the modification with the appearance of new chemical functions after functionalization of the biochar BNM by iron to obtain the ferromagnetic biochar BNMF. For example, on the FTIR spectrum of the ferromagnetic biochar (BNMF), an intense peak centered around 540 cm^{-1} appears contrary to what is observed on the spectrum of the precursor biochar (BNM). This intense peak is characteristic of the stretching mode of the vibration of iron oxides (Fe-O). These results are similar to those obtained by Ngankam et al. [33].

Energy dispersive X-ray spectroscopy was also used to qualitatively and quantitatively highlight the chemical elements present in the biochars. The non-modified biochar, for example, contains the chemical elements carbon (68.3%) and oxygen (31.7%), (Figure 3A),

while the ferromagnetic biochar contains carbon (34.3%), oxygen (30.5%) and iron (35.2%), (Figure 3B). The circular diagrams presented in Figure 3A,B give the percentages of the major chemical elements present in the structure of each of these two materials. The EDX analysis revealed the coexistence of the elements Fe, O and C on the surface of the ferromagnetic biochar, suggesting the possible formation of iron oxides. This testifies to the successful functionalization of the precursor biochar BNM by iron in solution. This is reflected in the coating of the surface of the biochar by iron atoms following iron–oxygen interactions as confirmed by the FTIR analyses, with the formation of nanoparticles of iron oxides on the surface of the biochar.

The SEM images of the two samples show porous surfaces with granular morphology, with the particles agglomerated with each other. The SEM image of the ferromagnetic biochar shows a homogeneous surface, where the iron particles are indistinguishable from the components of the unmodified biochar. This highlights the fact that the functionalization of the biochar by iron did not really modify the surface properties of the resulting ferromagnetic biochar.

In order to understand the arrangement of iron in the BNM ferromagnetic biochar, a mapping study was carried out as shown in Figure 3B1 (B1: C, B2: O, B3: Fe). This study presents the distribution of carbon, oxygen and iron atoms in the BNM material. The surface mapping of the ferromagnetic biochar (Figure 3B1) shows a surface filled with iron oxide that covers the porous carbonaceous and oxygenated surface of the biochar. In addition, the presence of cavity-shaped pores on the surface of the biochar is favorable to the adsorption of iron particles during synthesis [34,35].

The XRD analysis of the BNM and BNMf samples is shown in Figure 4. The XRD pattern of the biochar (BNM) shows the absence of crystalline peaks compared to that of the BNMf sample. This means that biochar prepared from mango seeds using pyrolysis is mostly amorphous [36]. On the BNMf XRD model, crystalline peaks are distinctly observed at 2θ values of 30.2° , 35.5° , 43.3° , 53.7° and 57.2° , corresponding to the Miller indices (220), (311), (400), (422) and (511). These values are characteristic of the inverse cubic spinel group of magnetite [37]. The hydrothermal treatment applied to the biochar BNM during its modification by iron to prepare the ferromagnetic biochar structurally modified the amorphous structure of the BNM to obtain the ferromagnetic biochar BNMf of crystalline structure. The crystal structure obtained for the ferromagnetic biochar sample as well as its crystallinity were evidenced by the appearance of well-defined peaks visible on its X-ray diffractogram (red colored pattern) in Figure 4. The pattern of BNMf indicates that the preparation of the ferromagnetic biochar was successful with a structural and crystallographic reorganization of the resulting product.

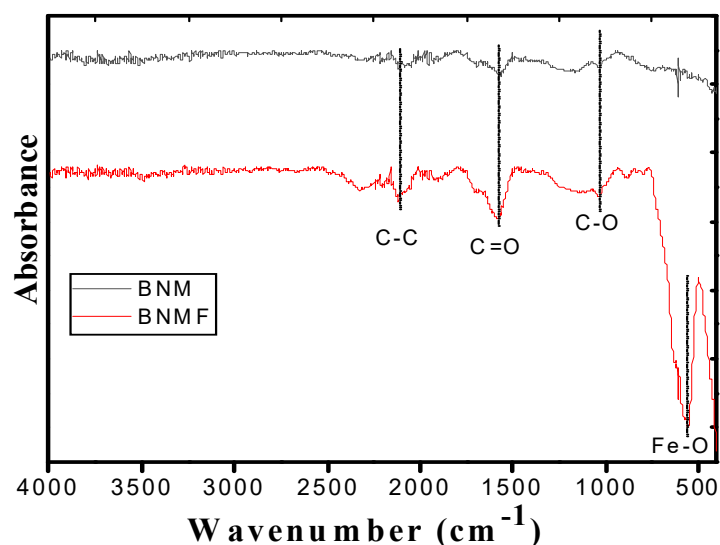


Figure 2. FTIR spectra of biochar (BNM) and ferromagnetic biochar (BNMF).

The elemental composition and semi-quantitative analysis of the non-modified biochar (BNM) and the ferromagnetic biochar (BNMF) are shown in the EDX spectra of Figure 3A,B. In these two figures, there is a notable difference in the two materials. In Figure 3A, it is observed that BNM contains carbon and oxygen. In Figure 3B, it can be seen that the BNMF, besides carbon and oxygen, also contains a high percentage of Fe (35.2%).

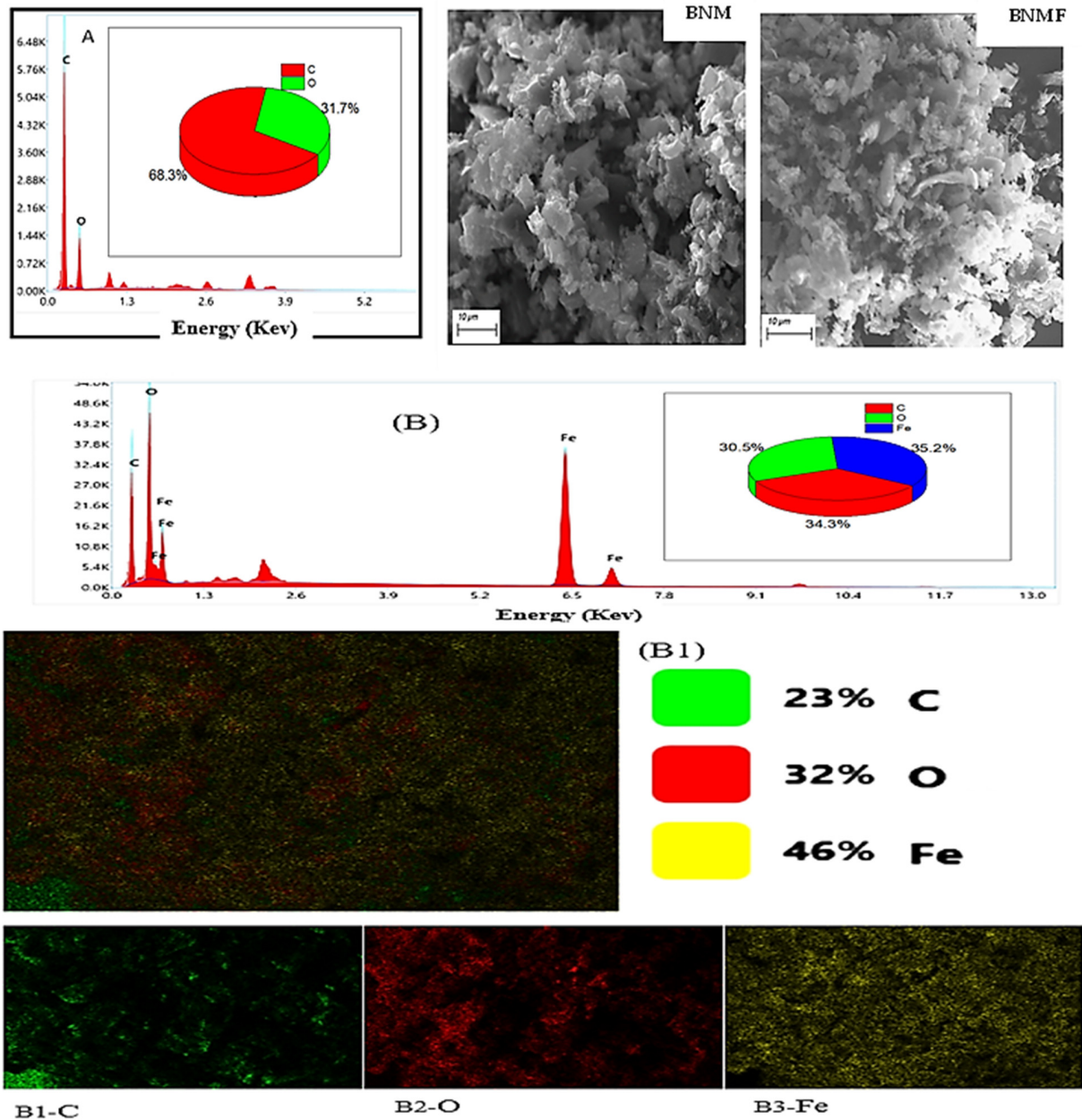


Figure 3. EDX images of non-modified biochar (A) and ferromagnetic biochar (B), SEM images of non-modified biochar (BNM) and ferromagnetic biochar (BNMF), elemental mapping for ferromagnetic biochar from image B1–B3.

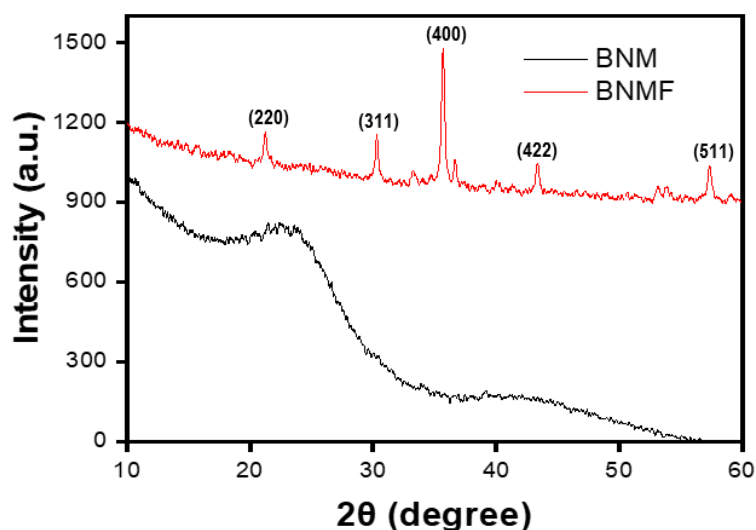


Figure 4. X-ray diffractograms of non-modified biochar (BNM) and ferromagnetic biochar (BNMF).

3.2. Degradation of Indigo Carmine in Aqueous Solution

3.2.1. Influence of the Type of Catalyst on the Degradation Process

The results obtained during the degradation of indigo carmine by the homogeneous and heterogeneous Fenton processes are shown in Figure 5.

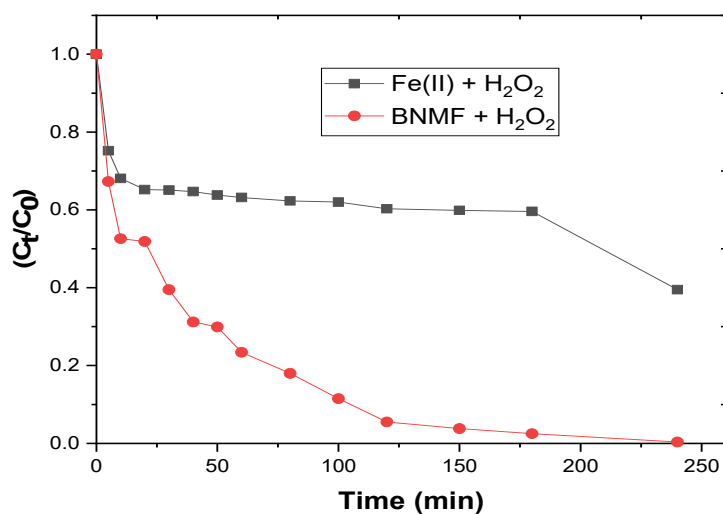


Figure 5. Influence of the presence of BNMF on the degradation of indigo carmine in comparison with the results obtained using Fe(II) in an oxygenated medium as catalyst.

The degradation of indigo carmine was studied using different methods, namely homogeneous ($\text{Fe}^{2+}/\text{H}_2\text{O}_2$) and heterogeneous (BNMF/ H_2O_2) Fenton processes in a solution of 100 mg/L of indigo carmine at pH 3. The results showed a percentage of degradation of indigo carmine of 99.66% in the presence of the ferromagnetic biochar as catalyst. This is due to the electron-rich biochar surface of the quinone groups, which facilitate ion exchange during catalysis [38], while that of the homogeneous Fenton process is only 60.50% after an equilibrium time of 4 h. The ferromagnetic biochar ensures a continuous and regulated flow with respect to Fe^{2+} during the Fenton reaction while the degradation in the absence of the ferromagnetic biochar quickly reaches equilibrium after about 1 h with a very low percentage of degradation. This rapid termination of the homogeneous Fenton reaction can be attributed to the decrease in iron concentration in the solution. These results are similar to those obtained by Ngankam et al. for the removal of methylene blue by the homogeneous and heterogeneous Fenton processes [33]. Since the highest percentage

of degradation was obtained using ferromagnetic biochar compared to $\text{Fe(II)/H}_2\text{O}_2$, the following experiments were conducted using ferromagnetic biochar (BNMF) as catalyst.

3.2.2. Influence of pH on the Degradation Process

The pH is one of the most important parameters affecting the Fenton process. The results obtained from the variation of the pH are presented in Figure 6.

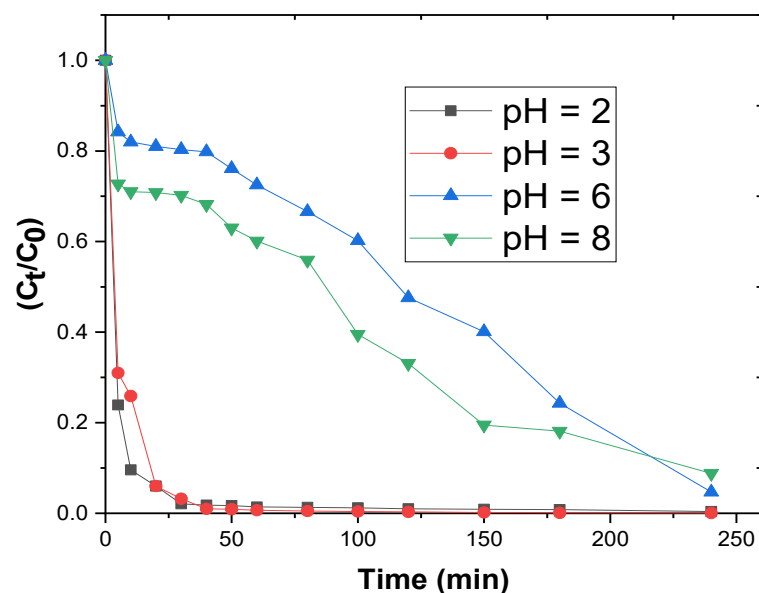


Figure 6. Effect of pH on the degradation of indigo carmine in aqueous solution.

The measurements of the concentration of indigo carmine were carried out using the UV-Vis set at the 612 nm wavelength. By adjusting the pH of the mixture to 3, a percentage degradation of 99.95% was obtained after 240 min of treatment. The decolorization of the dye was compared to those obtained for a pH of 2, 6 and 8. Some previous studies have shown that for pH values greater than 4, ferrous ions are unstable and tend to easily form complexable ferric ions in iron hydroxides [39,40]. The indigo carmine degradation experiments in the solution via the Fenton process were carried out using ferromagnetic biochar as catalyst, which contains a high concentration of iron as revealed by EDX analyses performed on this material. In the case of pH, the chemistry of iron requires that the Fenton reaction is carried out under acidic conditions (pH = 3–4) to avoid its precipitation in the form of hydroxide. At pH 3 (strongly acidic pH) and in the presence of H_2O_2 , ferric iron was the major dissolved iron species, and pH under acidic conditions maintains relatively high levels of dissolved iron in the aqueous solution. The higher iron concentration in the ferromagnetic biochar matrix or in the solution contributed to the efficient production of hydroxyl radicals and degradation of indigo carmine [41–44]. Dutta et al. in 2001 found that the optimum pH in the treatment of methylene blue by the Fenton process was between 2 and 3 [45]. Our results are also similar to those of Karale et al. [46], who found an optimal pH of 3 for the treatment of 2-aminopyridine by advanced oxidation using laterite. They showed that the low percentage of degradation at pH 2 and 2.5 was due to the trapping of H^+ ions from hydroxyl radicals and the inhibition of the formation of ferrous ions in solution [46].

3.2.3. Influence of H_2O_2 Concentration on the Degradation Process

Hydrogen peroxide (H_2O_2) is the source of HO^\bullet in the Fenton process. Therefore, its concentration will have a direct impact on the degradation of indigo carmine. The effect of the concentration of H_2O_2 on the degradation of indigo carmine is shown in Figure 7.

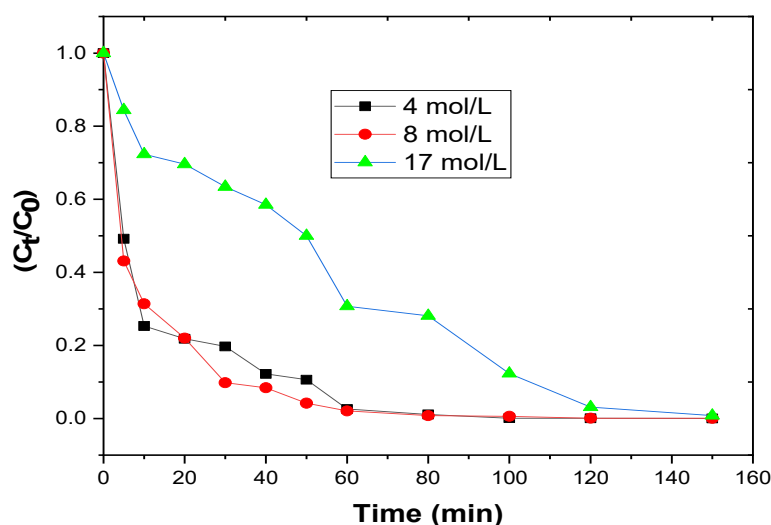


Figure 7. Effect of H_2O_2 concentration on the degradation of indigo carmine in the aqueous solution.

Figure 7 reveals that increasing the concentration of H_2O_2 from 8 to 17 mol/L leads to a corresponding increase in the degradation of the pollutant in the solution. This is consistent with the results reported in the literature [47–49]. Nevertheless, the surprisingly high removal percentage (99.97%) of the pollutant with a hydrogen peroxide concentration of 4 mol/L can be related to the fact that with a low H_2O_2 concentration, a limited amount of OH^\bullet is generated and the Fenton reaction does not come to an end. This leaves room for the pollutant to be adsorbed onto the surface of the BNMF instead. Therefore, Fenton degradation and adsorption synergy can be achieved using low concentrations of H_2O_2 in the presence of heterogeneous catalyst supports. The H_2O_2 plays an important role in the degradation process of indigo carmine. The Fenton reaction involves the generation of hydroxyl radicals by the catalytic decomposition of hydrogen peroxide in the presence of ferrous iron. A greater amount of iron should therefore lead to the production of many more OH^\bullet in the presence of hydrogen peroxide. This reaction is based on the electron transfer reactions between H_2O_2 and ferrous ions. During the process, regeneration of the ferrous ion in the presence of hydrogen peroxide and hydroperoxyl radical takes place. These reactions are an advantage for the Fenton process in terms of additional degradation by ferrous ions, which allows the production of many more OH^\bullet radicals that will lead to further degradation of the organic molecules in the solution [50,51].

3.2.4. Influence of Light Intensity on the Degradation Process

The results obtained for the study of the influence of light on the degradation of indigo carmine are shown in Figure 8.

Figure 8 above shows that when irradiating the reaction medium with a 100 W lamp, a higher percentage of degradation (98.20%) is achieved compared to daylight (90.34%). However, these results show that daylight also contributes significantly to the degradation of the pollutant. On the other hand, the lowest percentage of degradation is obtained in the dark. Indeed, the 100 W radiation produces more HO^\bullet radicals by initiating the direct photolysis of H_2O_2 and the photoreduction of Fe^{3+} to Fe^{2+} , which generates more HO^\bullet for the Fenton reaction.

The Fenton reaction is optimal in the presence of hydrogen peroxide and leads to the cleavage of chemical bonds of H_2O_2 by ferrous or ferric ions (Fe^{2+} and Fe^{3+} , respectively). The presence of H_2O_2 is therefore essential during the Fenton process for the generation of more HO^\bullet radicals, which allow the complete mineralization of complex and reactive organic substances such as dyes [52]. Under the effect of light irradiation, the heterogeneous Fenton process produces HO^\bullet radicals. The radical formation equations are denoted in Equations (7)–(11), which occur simultaneously. The reactions take place mainly on the surface of the ferromagnetic catalyst (BNMF biochar). In the heterogeneous Fenton

process, the particles of iron oxides (Fe_2O_3) and/or ferric ions covering the surface of the ferromagnetic biochar react with molecules of hydrogen peroxide and form complexes (Equation (7)). Thereafter, charge transfers between the ligands and the central metal take place and give rise to the formation of transient intermediate complexes with the structure: ($\equiv \text{Fe}^{\text{II}}\cdot\text{O}_2\text{H}$) (Equation (8)). Subsequently, these transient complexes dissociate and lead to the formation of hydroperoxyl $\text{HO}_2\cdot$ radicals and the generation of iron (II) species (Equation (9)). In the Equation (10), the iron (II) species previously formed interact with the molecules of hydrogen peroxide in the solution, allowing the formation of $\text{HO}\cdot$ hydroxyl radicals [52–54]. Thus, the $\text{HO}\cdot$ radicals formed lead to the degradation and mineralization of indigo carmine molecules in the solution. At the end of the process, the catalyst (BNMF) is regenerated and an optimal degradation of the indigo carmine (IC) molecules leads to the production of carbon dioxide and water molecules as reaction products (Equation (11)).

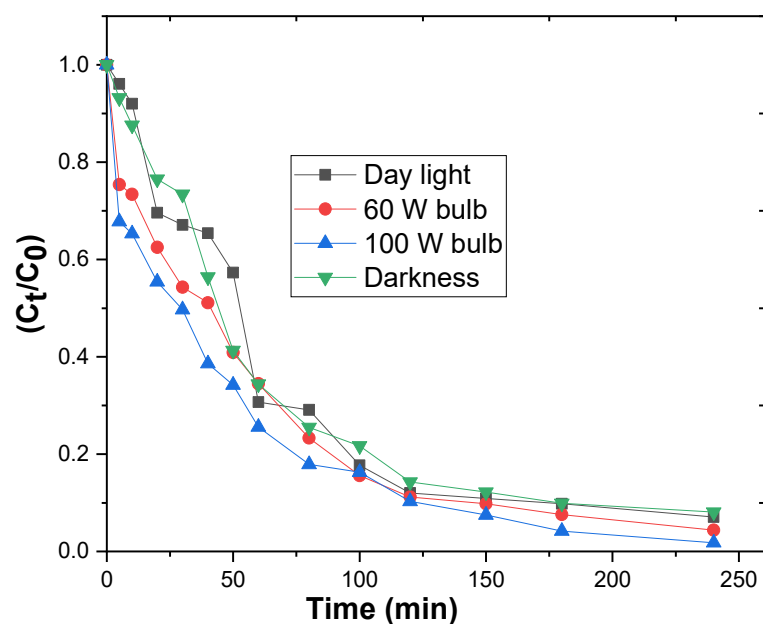
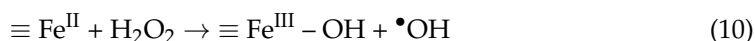
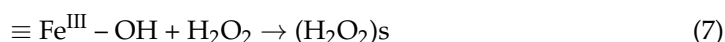


Figure 8. Effect of light intensity on indigo carmine degradation in the aqueous solution.

3.3. Kinetic Studies of the Degradation of Indigo Carmine

To describe the degradation kinetics of indigo carmine in the aqueous solution, first- and second-order kinetic models were used. Subsequently, the first- and second-order rate constants and half-lives of the Fenton reactions were determined. Figure 9 presents the linear regression plots of the first-order kinetics of indigo carmine degradation under the influence of pH (a), light intensity (b) and H_2O_2 concentration (c), while Table 1 summarizes the kinetic parameters associated with the degradation process considering the first-order kinetic model.

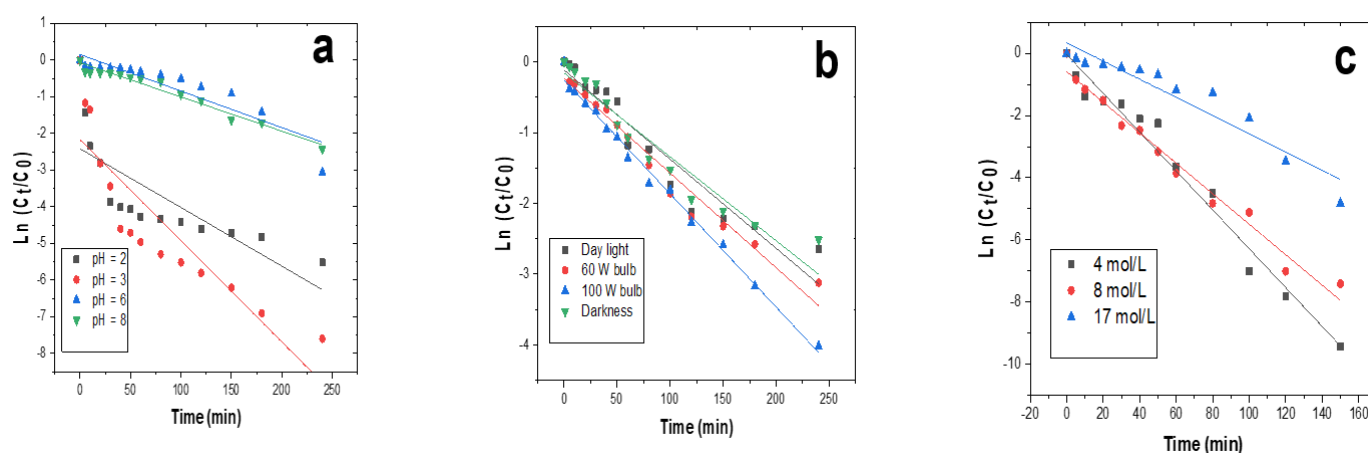


Figure 9. Linear regression plots of the first-order kinetics of indigo carmine degradation reactions under the influence of pH (a), light intensity (b) and H_2O_2 concentration (c).

Table 1. First-order rate constants and half-lives for degradation of indigo carmine.

Parameters	Variables	R^2	k (min^{-1})	$t_{1/2}$ (min)
pH	2	0.63	0.0162	42.59
	3	0.78	0.0271	25.46
	6	0.93	0.0115	60.00
	8	0.93	0.0114	60.52
Concentration of H_2O_2 (mol/L)	4	0.97	0.0615	11.21
	8	0.98	0.0478	14.43
	17	0.90	0.0295	23.38
Intensity of the light	Day light	0.93	0.0119	58.98
	60 W bulb	0.97	0.0132	52.27
	100 W bulb	0.99	0.0158	43.67
	Darkness	0.93	0.0119	57.88

For the first-order kinetics, the higher the value of the rate constant (k), the shorter the half-life ($t_{1/2}$) and the faster the degradation of the pollutant. By varying the pH of the medium, the fastest degradation rate is reached at pH 3 followed by pH 2. Indeed, at these pH values, there is a higher protonation of the aqueous medium, which favors the generation of more hydroxyl radicals to degrade the pollutant [33]. The correlation coefficient R^2 values obtained at these pH values are less than 0.9 and therefore the first-order rate law cannot be used to describe the degradation of indigo carmine in the presence of ferromagnetic biochar at pH 2 and 3 (Table 1). For the other conditions, this model seems to be appropriate for describing the kinetics of the degradation process with significantly higher R^2 values. The value of R^2 close to unity is obtained with a hydrogen peroxide concentration of 8 mol/L, indicating the adequacy of the first-order rate law to describe the kinetics of degradation with this concentration. We also note that degradation at a concentration of 4 mol/L has a half-life of only 11.21 min (Table 1), which means that the elimination of the pollutant is very rapid at this concentration thanks to the synergy of degradation and Fenton adsorption involved. The kinetic studies under the influence of light reveal that the degradation is faster with a 100 W bulb as the source of radiation and slower in total darkness. The R^2 with the 100 W bulb is close to unity and therefore degradation follows the first-order kinetics with the 100 W bulb.

Figure 10 below displays the linear regression plots of the second-order kinetics of the indigo carmine degradation reactions under the influence of pH (a), light intensity (b) and H_2O_2 concentration (c), while Table 2 summarizes the kinetic parameters associated with the degradation process considering the second-order kinetic model.

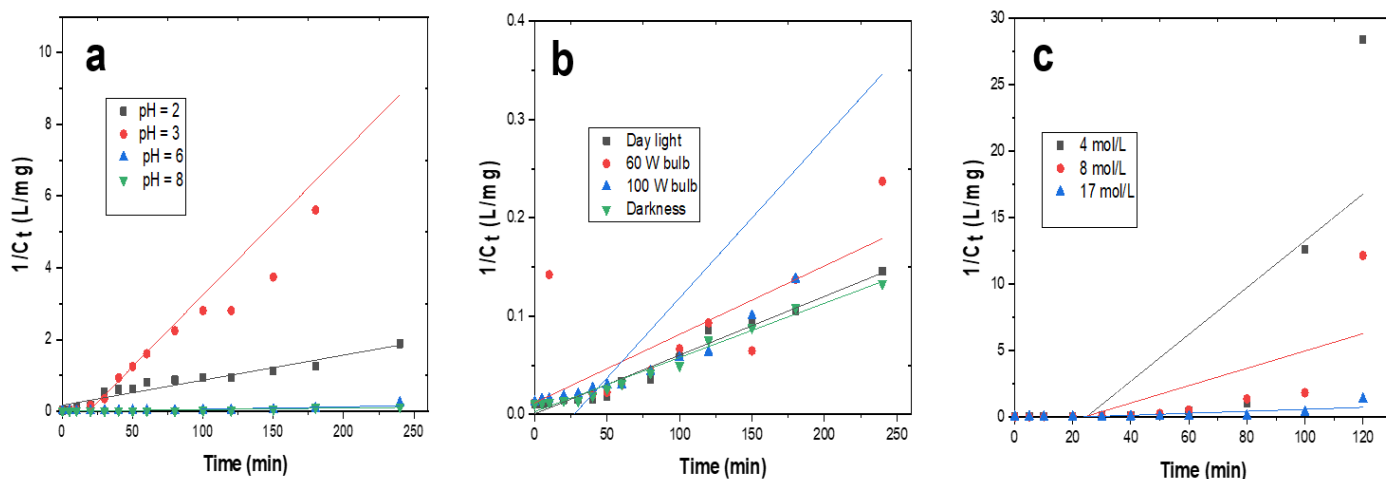


Figure 10. Linear regression plots of the second-order kinetics of indigo carmine degradation reactions under the influence of pH (a), light intensity (b) and H₂O₂ concentration (c).

Table 2. Second-order rate constants for indigo carmine degradation.

Parameters	Variables	R ²	k (dm ³ /mol·min)	t _{1/2} (min)
pH	2	0.930	0.011	1.075
	3	0.921	0.088	0.129
	6	0.880	0.001	18.796
	8	0.880	0.001	17.820
Concentration H ₂ O ₂ (mol/L)	4	0.538	0.622	0.022
	8	0.696	0.103	0.106
	17	0.554	0.006	1.891
Intensity of the light	Day light	0.968	0.001	18.331
	60 W bulb	0.938	0.001	14.930
	100 W bulb	0.785	0.002	5.739
	Darkness	0.981	0.001	18.911

The values of R² close to unity are obtained for pH values 2 and 3 with second-order kinetics. The fastest degradation rate is achieved at pH 3 with a half-life of only 0.1294 min. By varying the concentration of hydrogen peroxide, the fastest decolorization rate is achieved at 4 mol/L. The R² values at the concentration values 4, 8 and 17 mol/L are less than 0.9 and therefore the second-order rate law cannot be used to describe the degradation of indigo carmine in the presence of ferromagnetic biochar at these H₂O₂ concentration values. Under the effect of light, the second-order kinetic model also reveals how fast the degradation with a 100 W bulb is and how slow it is in the dark. When a light source is present, the photo-Fenton rate has been reported to be positively enhanced compared to the dark condition. This is mainly due to the regeneration of Fe²⁺ from the photochemical effect of light and the simultaneous generation of OH[•] radicals in the system. In the Fenton reaction, the ferrous and/or ferric cation catalytically decomposes the hydrogen peroxide to generate powerful oxidizing agents, capable of rapidly degrading a number of organic and inorganic substances. Light is therefore a determining parameter, which makes it possible to accelerate the degradation of organic molecules in the solution by the Fenton process and thus to increase the rate constants and reduce the catalytic reaction times associated with the Fenton processes involved [55,56].

3.4. Plausible Mechanism of Indigo Carmine Degradation

A plausible reaction mechanism for the degradation of indigo carmine in the aqueous solution is illustrated in the reaction scheme in Figure 11 as proposed by Ramos and co-workers [51].

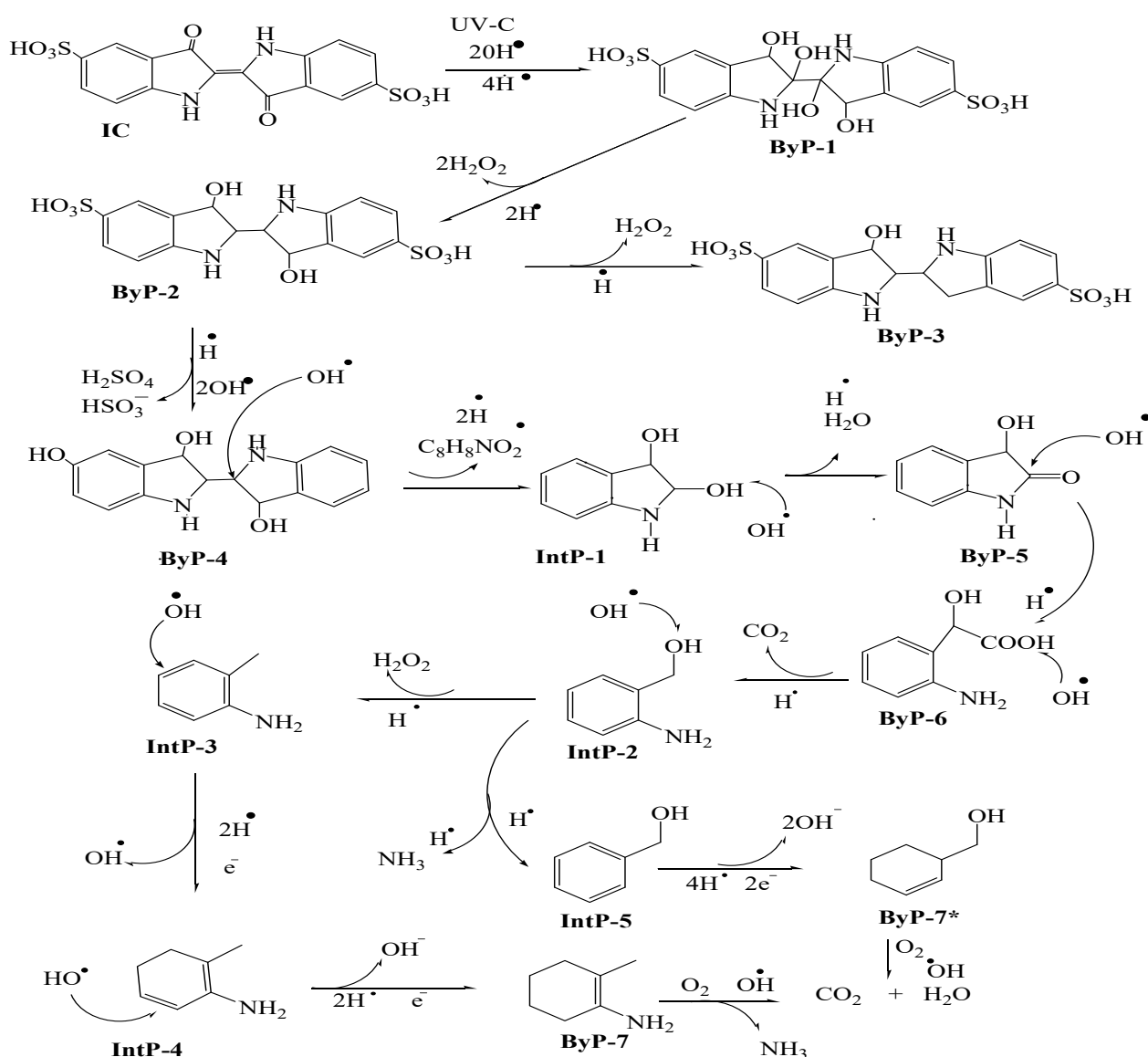


Figure 11. Mechanism of indigo carmine degradation via the Fenton process.

The reaction scheme described above for the mechanism of degradation of indigo carmine by the photo-Fenton process shows the formation of the reaction intermediates **ByP-1**: 2,2,3,3'-tetrahydro-5'-sulfo-2,2,3,3'-tetrahydropyridine-1,1'-[2,2'-bindole]-5-sulfonate; **ByP-2**: 3,3'-dihydroxy-2,2',3,3'-tetrahydro-1H,1'-[2,2'-bindole]-5,5'-disulfonic acid; **ByP-3**: 3-hydroxy-2,2,3,3'-tetrahydro-1H,1'-[2,2'-bindole]-5,5'-disulfonic acid; **ByP-4**: 2,2',3,3'-tetrahydro-1H,1'-[2,2'-bindole]-3,3',5'-triol; **ByP-5**: 3-hydroxy-1,3-dihydro-2H-indol-2-one; **ByP-6**: 2-(2-aminophenyl)-2-hydroxyacetic acid; **ByP-7**: 2-methylcyclohex-1-en-1-amine; **IntP-1**: 2,3-dihydro-1H-indole-2,3-diol; **ByP-7***: 2-cyclohexen-1-ylmethanol; **IntP-2**: 2-aminobenzyl alcohol; **IntP-3**: 2-methylaniline; **IntP-4**: methylcyclohexa-1,5-diene-1-amine; **IntP-5**: benzyl alcohol.

According to this mechanism, the degradation of indigo carmine under light irradiation in the presence of hydrogen peroxide begins with the breaking of the C=C double bond between the central carbons of the molecule, followed by a structural reorganization of the indigo carmine molecule with cleavage of the carbonyl functions of the molecule and their transformation into hydroxyl groups. The hydroxyl radicals interact with the carbons adjacent to those of the C=C double bond as well as with the two carbon atoms that constituted the previously cleaved C=C double bond. This process resulted in the formation of the reaction intermediate ByP-1. The next step in indigo carmine degradation

occurs when the OH^\bullet radicals approach the ByP-1 molecule and promote the abstraction of the hydroxyl groups previously attached to the two adjacent and central carbon atoms to generate H_2O_2 [11]. Subsequently, H^\bullet radicals are grafted onto the molecular intermediate leading to the reaction intermediate indexed ByP-2. The presence of more H^\bullet radicals in the presence of the ByP-2 intermediate favors the production of ByP-3 by cleavage of one of the C–OH bonds, followed by covalent interactions between the carbon radical formed and the proton radicals in the reaction medium. During this process, molecules of hydrogen peroxides (H_2O_2) are released [57].

The conversion of ByP-2 to ByP-4 occurs after the removal of the two bisulfite groups in a process that could occur via two pathways. The first pathway includes the removal of the HSO_3^\bullet radicals from the indigo carmine molecule by the interactions of the OH^\bullet radicals with the sulfur atom, resulting in the cleavage of the S–C bond, the release of sulfuric acid and the formation of a carbon radical. Another pathway results in the formation of a bond between the OH^\bullet radicals and the carbon of the S–C bond, resulting in the removal of HSO_3^- and the formation of a hydroxyl group [57–60]. Subsequently, the attack of the central C–C bond of the ByP-4 intermediate by the hydroxyl radical results in the cleavage of the C–C bond and the formation of a new C–OH bond, generating the IntP-1 intermediate and a radical $\text{C}_8\text{H}_8\text{NO}_2^\bullet$. Bonding between the newly formed hydroxyl group and the OH^\bullet radicals results in the subtraction of the H^\bullet radical and H_2O molecules with the generation of a carbonyl group giving rise to the dioxindole intermediate ByP-5 [58,61,62].

The interaction of the carbonyl carbon of ByP-5 with OH^\bullet causes the cleavage of the N–C bond, followed by the subsequent connection of H^\bullet to nitrogen resulting in the formation of ByP-6. In the sequel, the hydrogen from the –COOH functional group of ByP-6 is extracted by the attack of OH^\bullet , resulting in the formation of a second C–O bond with the subsequent removal of carbon dioxide and addition of H^\bullet to produce the reaction intermediate IntP-2. The reaction allowing the conversion of IntP-2 into IntP-3 occurs via the abstraction of the OH group by the action of OH^\bullet following the cleavage of the C–OH bond in the IntP-2 molecule [51]. Subsequently, the attack of the aromatic nucleus of IntP-3 by hydroxyl radicals leads to the removal of electrons with the formation of a carbon radical and a carbanion, which, after the addition of H^\bullet forms IntP-4. The mechanism leading to the conversion of the reaction intermediate indexed IntP-4 to that named ByP-7 is similar to that leading to the conversion of IntP-3 to IntP-4. An alternative route from IntP-2 allows the cleavage of the NH_2 group of this reaction intermediate, thus generating the benzyl alcohol IntP-5. In this case, the release of electrons from the aromatic ring of IntP-5 occurs as described for IntP-3, thus giving rise to the formation of the reaction intermediate ByP-7*. Finally, in the presence of oxygen, the OH^\bullet radicals promote the degradation and mineralization of ByP-7 and ByP-7* with the formation of carbon dioxide (CO_2) and water (H_2O) as reaction products [51].

4. Conclusions

Ferromagnetic biochar was prepared by a hydrothermal method using biochar obtained from the pyrolysis of mango seeds. The physico-chemical characterizations carried out on the prepared materials (BNM and BNMF) showed a good dispersion of the magnetite particles on the surface of the ferromagnetic biochar with a structural reorganization in the crystalline matrix of the ferromagnetic biochar, compared to the amorphous structure of the precursor biochar. Ferromagnetic biochar has been shown to be very useful in the degradation of indigo carmine in aqueous media using the heterogeneous Fenton process. The use of H_2O_2 as an oxidizing agent strongly favored the degradation. The variation of the parameters revealed that the optimal conditions for the degradation of indigo carmine include a pH range between 2 and 3, and irradiation from a 100 W electric lamp. Regarding the H_2O_2 concentration, it was recorded during the experiment that a maximum of pollutant can be eliminated from an aqueous solution by using a concentration of 4 mol/L. Kinetic studies have also shown that the degradation rate is fastest with a pH of 3, a 100 W electric lamp and a hydrogen peroxide concentration of 4 mol/L. Therefore, it can be conclusively stated that ferromagnetic

biochar can be prepared from agricultural waste to effectively remove indigo carmine from wastewater using the Fenton process. Percentages of degradation greater than 90% have been obtained under certain experimental conditions. Experimental work on real industrial effluents is envisaged in addition to the work already carried out in this study. However, in view of the results already obtained it appears that water samples containing indigo carmine, which is relatively toxic for fauna and flora and having effects on human health, can be effectively processed and reused for other major needs.

Author Contributions: Conceptualization, A.B., G.N.-A.N. and S.G.A.; methodology, A.B. and D.R.T.T.; software, G.T.K., D.R.T.T., C.G.F. and A.K.T.; validation, A.B., I.-H.T.K., C.S.N., G.N.-A.N. and S.G.A.; investigation, A.B., S.G.M.M., J.N.N., G.T.K., C.G.F., I.-H.T.K., C.S.N., D.R.T.T. and A.K.T.; writing—original draft preparation, A.B., S.G.M.M. and J.N.N.; writing—review and editing, D.R.T.T., C.G.F. and A.K.T.; supervision, G.N.-A.N. and S.G.A.; project administration, G.N.-A.N. and S.G.A. All authors have read and agreed to the published version of the manuscript.

Funding: This research was financially supported by the German Academic Exchange Service (DAAD) and the Research Unit of Noxious Chemistry and Environmental Engineering (RUNOCHEE) of the University of Dschang (Cameroon).

Data Availability Statement: Not applicable.

Acknowledgments: C.G.F. and A.K.T. thank the German Academic Exchange Service (DAAD) for financial support.

Conflicts of Interest: The authors declare no conflict of interest.

References

1. Kuete, I.-H.T.; Tchuifon, D.R.T.; Ndifor-Angwafor, G.N.; Kamdem, A.T.; Anagho, S.G. Kinetic, Isotherm and Thermodynamic Studies of the Adsorption of Thymol Blue onto Powdered Activated Carbons from Garcinia Cola Nut Shells Impregnated with H_3PO_4 and KOH: Non-Linear Regression Analysis. *JEAS* **2020**, *10*, 1–27. [\[CrossRef\]](#)
2. Ngaha, M.C.D.; Njanja, E.; Doungmo, G.; Tamo Kamdem, A.; Tonle, I.K. Indigo Carmine and 2,6-Dichlorophenolindophenol Removal Using Cetyltrimethylammonium Bromide-Modified Palm Oil Fiber: Adsorption Isotherms and Mass Transfer Kinetics. *Int. J. Biomater.* **2019**, *2019*, 6862825. [\[CrossRef\]](#) [\[PubMed\]](#)
3. Alsukaibi, A.K.D. Various Approaches for the Detoxification of Toxic Dyes in Wastewater. *Processes* **2022**, *10*, 1968. [\[CrossRef\]](#)
4. Ngouoko, J.J.K.; Tajeu, K.Y.; Temgoua, R.C.T.; Doungmo, G.; Doench, I.; Tamo, A.K.; Kamgaing, T.; Osorio-Madrado, A.; Tonle, I.K. Hydroxyapatite/L-Lysine Composite Coating as Glassy Carbon Electrode Modifier for the Analysis and Detection of Nile Blue A. *Materials* **2022**, *15*, 4262. [\[CrossRef\]](#)
5. Ngouoko, J.J.K.; Tajeu, K.Y.; Fotsop, C.G.; Tamo, A.K.; Doungmo, G.; Temgoua, R.C.T.; Kamgaing, T.; Tonle, I.K. Calcium Carbonate Originating from Snail Shells for Synthesis of Hydroxyapatite/L-Lysine Composite: Characterization and Application to the Electroanalysis of Toluidine Blue. *Crystals* **2022**, *12*, 1189. [\[CrossRef\]](#)
6. Nindjio, G.F.K.; Tagne, R.F.T.; Jiokeng, S.L.Z.; Fotsop, C.G.; Bopda, A.; Doungmo, G.; Temgoua, R.C.T.; Doench, I.; Njoyim, E.T.; Tamo, A.K.; et al. Lignocellulosic-Based Materials from Bean and Pistachio Pod Wastes for Dye-Contaminated Water Treatment: Optimization and Modeling of Indigo Carmine Sorption. *Polymers* **2022**, *14*, 3776. [\[CrossRef\]](#)
7. Donlifack Atemkeng, C.; Tamo, A.K.; Doungmo, G.; Amola, L.A.; Kouanang Ngouoko, J.J.; Kamgaing, T. Thermodynamic, Nonlinear Kinetic, and Isotherm Studies of Bisphenol A Uptake onto Chemically Activated Carbons Derived from Safou (*Dacryodes Edulis*) Seeds. *J. Chem.* **2022**, *2022*, 1–17. [\[CrossRef\]](#)
8. Hakeem, K.R.; Bhat, R.A.; Qadri, H. (Eds.) *Bioremediation and Biotechnology*; Springer International Publishing: Cham, Switzerland, 2020; ISBN 978-3-030-35690-3.
9. Genázio Pereira, P.C.; Reimão, R.V.; Pavesi, T.; Saggiaro, E.M.; Moreira, J.C.; Veríssimo Correia, F. Lethal and Sub-Lethal Evaluation of Indigo Carmine Dye and Byproducts after TiO_2 Photocatalysis in the Immune System of Eisenia Andrei Earthworms. *Ecotoxicol. Environ. Saf.* **2017**, *143*, 275–282. [\[CrossRef\]](#)
10. Debina, B.; Eric, S.N.; Fotio, D.; Arnaud, K.T.; Lemankreo, D.-Y.; Rahman, A.N. Adsorption of Indigo Carmine Dye by Composite Activated Carbons Prepared from Plastic Waste (PET) and Banana Pseudo Stem. *MSCE* **2020**, *8*, 39–55. [\[CrossRef\]](#)
11. Ortiz, E.; Gómez-Chávez, V.; Cortés-Romero, C.M.; Solís, H.; Ruiz-Ramos, R.; Loera-Serna, S. Degradation of Indigo Carmine Using Advanced Oxidation Processes: Synergy Effects and Toxicological Study. *JEP* **2016**, *7*, 1693–1706. [\[CrossRef\]](#)
12. Ahmad, M.B.; Soomro, U.; Muqet, M.; Ahmed, Z. Adsorption of Indigo Carmine Dye onto the Surface-Modified Adsorbent Prepared from Municipal Waste and Simulation Using Deep Neural Network. *J. Hazard. Mater.* **2021**, *408*, 124433. [\[CrossRef\]](#) [\[PubMed\]](#)

13. Ahmed, M.; Mavukkandy, M.O.; Giwa, A.; Elektorowicz, M.; Katsou, E.; Khelifi, O.; Naddeo, V.; Hasan, S.W. Recent Developments in Hazardous Pollutants Removal from Wastewater and Water Reuse within a Circular Economy. *npj Clean Water* **2022**, *5*, 109. [[CrossRef](#)]
14. Li, Z.; Sun, Y.; Liu, D.; Yi, M.; Chang, F.; Li, H.; Du, Y. A Review of Sulfate Radical-Based and Singlet Oxygen-Based Advanced Oxidation Technologies: Recent Advances and Prospects. *Catalysts* **2022**, *12*, 1092. [[CrossRef](#)]
15. Bustillo-Lecompte, C. (Ed.) *Advanced Oxidation Processes—Applications, Trends, and Prospects*; IntechOpen: London, UK, 2020; ISBN 978-1-78984-890-8.
16. Xu, M.; Wu, C.; Zhou, Y. Advancements in the Fenton Process for Wastewater Treatment. In *Advanced Oxidation Processes—Applications, Trends, and Prospects*; Bustillo-Lecompte, C., Ed.; IntechOpen: London, UK, 2020; ISBN 978-1-78984-890-8.
17. Krupińska, I. Impact of the Oxidant Type on the Efficiency of the Oxidation and Removal of Iron Compounds from Groundwater Containing Humic Substances. *Molecules* **2020**, *25*, 3380. [[CrossRef](#)] [[PubMed](#)]
18. Lyu, L.; Zhang, L.; He, G.; He, H.; Hu, C. Selective H₂O₂ Conversion to Hydroxyl Radicals in the Electron-Rich Area of Hydroxylated C-g-C₃N₄/CuCo–Al₂O₃. *J. Mater. Chem. A* **2017**, *5*, 7153–7164. [[CrossRef](#)]
19. Gasim, M.F.; Choong, Z.-Y.; Koo, P.-L.; Low, S.-C.; Abdurahman, M.-H.; Ho, Y.-C.; Mohamad, M.; Suryawan, I.W.K.; Lim, J.-W.; Oh, W.-D. Application of Biochar as Functional Material for Remediation of Organic Pollutants in Water: An Overview. *Catalysts* **2022**, *12*, 210. [[CrossRef](#)]
20. Tu, Y.; Peng, Z.; Xu, P.; Lin, H.; Wu, X.; Yang, L.; Huang, J. Characterization and Application of Magnetic Biochars from Corn Stalk by Pyrolysis and Hydrothermal Treatment. *BioResources* **2016**, *12*, 1077–1089. [[CrossRef](#)]
21. Jia, L.; Yu, Y.; Li, Z.-P.; Qin, S.-N.; Guo, J.-R.; Zhang, Y.-Q.; Wang, J.-C.; Zhang, J.-C.; Fan, B.-G.; Jin, Y. Study on the Hg⁰ Removal Characteristics and Synergistic Mechanism of Iron-Based Modified Biochar Doped with Multiple Metals. *Bioresour. Technol.* **2021**, *332*, 125086. [[CrossRef](#)]
22. Ozel, F.; Kockar, H. Growth and Characterizations of Magnetic Nanoparticles under Hydrothermal Conditions: Reaction Time and Temperature. *J. Magn. Magn. Mater.* **2015**, *373*, 213–216. [[CrossRef](#)]
23. Gan, Y.X.; Jayatissa, A.H.; Yu, Z.; Chen, X.; Li, M. Hydrothermal Synthesis of Nanomaterials. *J. Nanomater.* **2020**, *2020*, 8917013. [[CrossRef](#)]
24. Kumar, P.; Joshi, L. Pollution Caused by Agricultural Waste Burning and Possible Alternate Uses of Crop Stubble: A Case Study of Punjab. In *Knowledge Systems of Societies for Adaptation and Mitigation of Impacts of Climate Change*; Nautiyal, S., Rao, K.S., Kaechele, H., Raju, K.V., Schaldach, R., Eds.; Environmental Science and Engineering; Springer: Berlin/Heidelberg, Germany, 2013; pp. 367–385. ISBN 978-3-642-36142-5.
25. Usmani, M.; Kondal, A.; Wang, J.; Jutla, A. Environmental Association of Burning Agricultural Biomass in the Indus River Basin. *GeoHealth* **2020**, *4*, e2020GH000281. [[CrossRef](#)]
26. Gupta, S. Agriculture Crop Residue Burning and Its Consequences on Respiration Health of School-Going Children. *Glob. Pediatr. Health* **2019**, *6*, 2333794X1987467. [[CrossRef](#)]
27. Al-Tohamy, R.; Ali, S.S.; Li, F.; Okasha, K.M.; Mahmoud, Y.A.-G.; Elsamahy, T.; Jiao, H.; Fu, Y.; Sun, J. A Critical Review on the Treatment of Dye-Containing Wastewater: Ecotoxicological and Health Concerns of Textile Dyes and Possible Remediation Approaches for Environmental Safety. *Ecotoxicol. Environ. Saf.* **2022**, *231*, 113160. [[CrossRef](#)]
28. Lall, A.; Kamdem Tamo, A.; Doench, I.; David, L.; Nunes de Oliveira, P.; Gorzelanny, C.; Osorio-Madrado, A. Nanoparticles and Colloidal Hydrogels of Chitosan-Caseinate Polyelectrolyte Complexes for Drug-Controlled Release Applications. *Int. J. Mol. Sci.* **2020**, *21*, 5602. [[CrossRef](#)]
29. Deussi Ngaha, M.C.; Kougoum Tchieda, V.; Kamdem Tamo, A.; Doungmo, G.; Njanja, E.; Kenfack Tonle, I. Aminoalcohol-functionalization of Alkali Palm Oil Fiber and Application as Electrochemical Sensor for 2-nitrophenol Determination. *Electroanalysis* **2022**, *9*, 5222. [[CrossRef](#)]
30. Marquez-Bravo, S.; Doench, I.; Molina, P.; Bentley, F.E.; Tamo, A.K.; Passieux, R.; Lossada, F.; David, L.; Osorio-Madrado, A. Functional Bionanocomposite Fibers of Chitosan Filled with Cellulose Nanofibers Obtained by Gel Spinning. *Polymers* **2021**, *13*, 1563. [[CrossRef](#)]
31. Kamdem Tamo, A.; Doench, I.; Morales Helguera, A.; Hoenders, D.; Walther, A.; Madrazo, A.O. Biodegradation of Crystalline Cellulose Nanofibers by Means of Enzyme Immobilized-Alginate Beads and Microparticles. *Polymers* **2020**, *12*, 1522. [[CrossRef](#)]
32. Djouonkep, L.D.W.; Tamo, A.K.; Doench, I.; Selabi, N.B.S.; Ilunga, E.M.; Lenwoue, A.R.K.; Gauthier, M.; Cheng, Z.; Osorio-Madrado, A. Synthesis of High Performance Thiophene-Aromatic Polyesters from Bio-Sourced Organic Acids and Polysaccharide-Derived Diol: Characterization and Degradability Studies. *Molecules* **2022**, *27*, 325. [[CrossRef](#)]
33. Ngankam, E.S.; Dai-Yang, L.; Debina, B.; Baçaoui, A.; Yaacoubi, A.; Rahman, A.N. Preparation and Characterization of Magnetic Banana Peels Biochar for Fenton Degradation of Methylene Blue. *MSA* **2020**, *11*, 382–400. [[CrossRef](#)]
34. Peng, Z.; Fan, Z.; Chen, X.; Zhou, X.; Gao, Z.F.; Deng, S.; Wan, S.; Lv, X.; Shi, Y.; Han, W. Fabrication of Nano Iron Oxide-Modified Biochar from Co-Hydrothermal Carbonization of Microalgae and Fe(II) Salt for Efficient Removal of Rhodamine B. *Nanomaterials* **2022**, *12*, 2271. [[CrossRef](#)]
35. Zhou, W.; Rajic, L.; Chen, L.; Kou, K.; Ding, Y.; Meng, X.; Wang, Y.; Mulaw, B.; Gao, J.; Qin, Y.; et al. Activated Carbon as Effective Cathode Material in Iron-Free Electro-Fenton Process: Integrated H₂O₂ Electrogeneration, Activation, and Pollutants Adsorption. *Electrochim. Acta* **2019**, *296*, 317–326. [[CrossRef](#)] [[PubMed](#)]

36. Armynah, B.; Atika; Djafar, Z.; Piarah, W.H.; Tahir, D. Analysis of Chemical and Physical Properties of Biochar from Rice Husk Biomass. *J. Phys. Conf. Ser.* **2018**, *979*, 012038. [[CrossRef](#)]
37. Hariani, P.L.; Faizal, M.; Ridwan; Marsi; Setiabudidaya, D. Removal of Procion Red MX-5B from Songket's Industrial Wastewater in South Sumatra Indonesia Using Activated Carbon-Fe₃O₄ Composite. *Sustain. Environ. Res.* **2018**, *28*, 158–164. [[CrossRef](#)]
38. Klüpfel, L.; Keiluweit, M.; Kleber, M.; Sander, M. Redox Properties of Plant Biomass-Derived Black Carbon (Biochar). *Environ. Sci. Technol.* **2014**, *48*, 5601–5611. [[CrossRef](#)] [[PubMed](#)]
39. Stefanoni, M.; Zhang, Z.; Angst, U.; Elsener, B. The Kinetic Competition between Transport and Oxidation of Ferrous Ions Governs Precipitation of Corrosion Products in Carbonated Concrete. *RILEM Tech. Lett.* **2018**, *3*, 8–16. [[CrossRef](#)]
40. Rezaei, F.; Vione, D. Effect of PH on Zero Valent Iron Performance in Heterogeneous Fenton and Fenton-Like Processes: A Review. *Molecules* **2018**, *23*, 3127. [[CrossRef](#)]
41. Zhang, Y.; Zhao, L.; Yang, Y.; Sun, P. Fenton-Like Oxidation of Antibiotic Ornidazole Using Biochar-Supported Nanoscale Zero-Valent Iron as Heterogeneous Hydrogen Peroxide Activator. *Int. J. Environ. Res. Public Health* **2020**, *17*, 1324. [[CrossRef](#)]
42. Ajibade, P.A.; Nnadozie, E.C. Synthesis and Structural Studies of Manganese Ferrite and Zinc Ferrite Nanocomposites and Their Use as Photoadsorbents for Indigo Carmine and Methylene Blue Dyes. *ACS Omega* **2020**, *5*, 32386–32394. [[CrossRef](#)]
43. Bae, S.; Kim, D.; Lee, W. Degradation of Diclofenac by Pyrite Catalyzed Fenton Oxidation. *Appl. Catal. B Environ.* **2013**, *134–135*, 93–102. [[CrossRef](#)]
44. Dias, F.F.; Oliveira, A.A.S.; Arcanjo, A.P.; Moura, F.C.C.; Pacheco, J.G.A. Residue-Based Iron Catalyst for the Degradation of Textile Dye via Heterogeneous Photo-Fenton. *Appl. Catal. B Environ.* **2016**, *186*, 136–142. [[CrossRef](#)]
45. Dutta, K.; Mukhopadhyay, S.; Bhattacharjee, S.; Chaudhuri, B. Chemical Oxidation of Methylene Blue Using a Fenton-like Reaction. *J. Hazard. Mater.* **2001**, *84*, 57–71. [[CrossRef](#)]
46. Karale, R.S.; Manu, B.; Shrihari, S. Fenton and Photo-Fenton Oxidation Processes for Degradation of 3-Aminopyridine from Water. *APCBEE Procedia* **2014**, *9*, 25–29. [[CrossRef](#)]
47. Wang, J.; Li, S.; Qin, Q.; Peng, C. Sustainable and Feasible Reagent-Free Electro-Fenton via Sequential Dual-Cathode Electrocatalysis. *Proc. Natl. Acad. Sci. USA* **2021**, *118*, e2108573118. [[CrossRef](#)]
48. Kousar, T.; Bokhari, T.H.; Altaf, A.; ul Haq, A.; Muneer, M.; Farhat, L.B.; Alwadai, N.; Alfryyan, N.; Jilani, M.I.; Iqbal, M.; et al. SnO₂/UV/H₂O₂ and TiO₂/UV/H₂O₂ Efficiency for the Degradation of Reactive Yellow 160A: By-Product Distribution, Cytotoxicity and Mutagenicity Evaluation. *Catalysts* **2022**, *12*, 553. [[CrossRef](#)]
49. Giwa, A.-R.A.; Bello, I.A.; Olabintan, A.B.; Bello, O.S.; Saleh, T.A. Kinetic and Thermodynamic Studies of Fenton Oxidative Decolorization of Methylene Blue. *Heliyon* **2020**, *6*, e04454. [[CrossRef](#)]
50. Liu, Y.; Zhao, Y.; Wang, J. Fenton/Fenton-like Processes with in-Situ Production of Hydrogen Peroxide/Hydroxyl Radical for Degradation of Emerging Contaminants: Advances and Prospects. *J. Hazard. Mater.* **2021**, *404*, 124191. [[CrossRef](#)]
51. Ramos, R.O.; Albuquerque, M.V.C.; Lopes, W.S.; Sousa, J.T.; Leite, V.D. Degradation of Indigo Carmine by Photo-Fenton, Fenton, H₂O₂/UV-C and Direct UV-C: Comparison of Pathways, Products and Kinetics. *J. Water Process Eng.* **2020**, *37*, 101535. [[CrossRef](#)]
52. Gallego-Ramírez, C.; Chica, E.; Rubio-Clemente, A. Coupling of Advanced Oxidation Technologies and Biochar for the Removal of Dyes in Water. *Water* **2022**, *14*, 2531. [[CrossRef](#)]
53. Zhou, L.; Shao, Y.; Liu, J.; Ye, Z.; Zhang, H.; Ma, J.; Jia, Y.; Gao, W.; Li, Y. Preparation and Characterization of Magnetic Porous Carbon Microspheres for Removal of Methylene Blue by a Heterogeneous Fenton Reaction. *ACS Appl. Mater. Interfaces* **2014**, *6*, 7275–7285. [[CrossRef](#)]
54. Thomas, N.; Dionysiou, D.D.; Pillai, S.C. Heterogeneous Fenton Catalysts: A Review of Recent Advances. *J. Hazard. Mater.* **2021**, *404*, 124082. [[CrossRef](#)]
55. Maezono, T.; Tokumura, M.; Sekine, M.; Kawase, Y. Hydroxyl Radical Concentration Profile in Photo-Fenton Oxidation Process: Generation and Consumption of Hydroxyl Radicals during the Discoloration of Azo-Dye Orange II. *Chemosphere* **2011**, *82*, 1422–1430. [[CrossRef](#)] [[PubMed](#)]
56. Hossain, M.F. Water. In *Sustainable Design and Build*; Elsevier: Amsterdam, The Netherlands, 2019; pp. 301–418. ISBN 978-0-12-816722-9.
57. Torres-Blancas, T.; Roa-Morales, G.; Barrera-Díaz, C.; Ureña-Nuñez, F.; Cruz-Olivares, J.; Balderas-Hernandez, P.; Natividad, R. Ozonation of Indigo Carmine Enhanced by Fe/ *Pimenta Dioica* L. Merrill Particles. *Int. J. Photoenergy* **2015**, *2015*, 608412. [[CrossRef](#)]
58. Bernal, M.; Romero, R.; Roa, G.; Barrera-Díaz, C.; Torres-Blancas, T.; Natividad, R. Ozonation of Indigo Carmine Catalyzed with Fe-Pillared Clay. *Int. J. Photoenergy* **2013**, *2013*, 918025. [[CrossRef](#)]
59. Palma-Goyes, R.E.; Silva-Agredo, J.; González, I.; Torres-Palma, R.A. Comparative Degradation of Indigo Carmine by Electrochemical Oxidation and Advanced Oxidation Processes. *Electrochim. Acta* **2014**, *140*, 427–433. [[CrossRef](#)]
60. Terres, J.; Battisti, R.; Andreus, J.; de Jesus, P.C. Decolorization and Degradation of Indigo Carmine Dye from Aqueous Solution Catalyzed by Horseradish Peroxidase. *Biocatal. Biotransform.* **2014**, *32*, 64–73. [[CrossRef](#)]
61. Li, H.; Li, Y.; Xiang, L.; Huang, Q.; Qiu, J.; Zhang, H.; Sivaiah, M.V.; Baron, F.; Barrault, J.; Petit, S.; et al. Heterogeneous Photo-Fenton Decolorization of Orange II over Al-Pillared Fe-Smectite: Response Surface Approach, Degradation Pathway, and Toxicity Evaluation. *J. Hazard. Mater.* **2015**, *287*, 32–41. [[CrossRef](#)]
62. Luan, J.; Chen, M.; Hu, W. Synthesis, Characterization and Photocatalytic Activity of New Photocatalyst ZnBiSbO₄ under Visible Light Irradiation. *Int. J. Mol. Sci.* **2014**, *15*, 9459–9480. [[CrossRef](#)]